The trisulfur radical ion S 3 •− controls platinum transport by hydrothermal fluids

Gleb S Pokrovski, Maria A Kokh, Elsa Desmaele, Clément Laskar, Elena F Bazarkina, Anastassia y Borisova, Denis Testemale, Jean-Louis F Hazemann, Rodolphe Vuilleumier, Guillaume Ferlat, et al.

PNAS
www.pnas.org

Main Manuscript for

The trisulfur radical ion $S_3^{\bullet-}$ controls platinum transport by hydrothermal fluids

Gleb S. Pokrovski[1,*], Maria A. Kokh[1,5], Elsa Desmaele[2], Clément Laskar[1], Elena F. Bazarkina[3,6], Anastassia Y. Borisova[1,7], Denis Testemale[3], Jean-Louis Hazemann[3], Rodolphe Vuilleumier[2], Guillaume Ferlat[4], and Antonino Marco Saitta[4]

[1]Experimental Géosciences Team (GeoExp), Géosciences Environnement Toulouse (GET), UMR 5563 CNRS, Université Paul Sabatier Toulouse III, IRD, CNES, Observatoire Midi-Pyrénées, 14 av. Edouard Belin, F-31400 Toulouse, France.

[2]PASTEUR, Département de Chimie, École Normale Supérieure, PSL University, Sorbonne Université, CNRS, F-75005 Paris, France.

[3]Université Grenoble Alpes, CNRS, Institut Néel, 25 av. des Martyrs, F-38042 Grenoble Cedex 9, France.

[4]Sorbonne Université, CNRS, UMR 7590, IMPMC, F-75005 Paris, France.

[5]Universität Potsdam, Institut für Geowissenschaften, Campus Golm, Haus 27, Karl-Liebknecht-Str. 24-25, D-14476 Potsdam, Germany.

[6]Institute of Geology of Ore Deposits, Petrography, Mineralogy and Geochemistry, Russian Academy of Sciences (IGEM RAS), 35, Staromonetny per., F-119017 Moscow, Russia.

[7]Geological Department, Lomonosov Moscow State University, Vorobievy Gory, Moscow, Russia

[*]G.S. Pokrovski, phones: +33-5-61-33-26-18; +33-6-20-34-72-62; E-mail: gleb.pokrovski@get.omp.eu; glebounet@gmail.com

Author contributions:
G.S.P. designed research and wrote the paper;, M.A.K., E.D., D.T., C.L., R.V. and G.S.P. performed experiments and modeling; C.L., E.F.B., A.Y.B., J-L.H., G.F. and A.M.S. contributed new reagents/analytical/computational tools; G.S.P., M.A.K., E.D. analyzed data; all authors contributed to data interpretation and manuscript preparation.

Competing Interest Statement: The authors declare no competing interests.

Classifications: Physical - Earth, Atmospheric and Planetary Science

Keywords: platinum, sulfur, hydrothermal fluid, platinum group elements, trisulfur ion

This PDF file includes:

Main Text (incl. abstract, significance statement, ms text, references and figure cations = 4700 words)
Figures 1 to 3 (uploaded separately)
References 1 to 33

PNAS MS# 2021-09768 Revision 1

Abstract (177 words):

Platinum group elements (PGE) are considered to be very poorly soluble in aqueous fluids in most natural hydrothermal-magmatic contexts and industrial processes. Here we combined in situ X-ray absorption spectroscopy and solubility experiments with atomistic and thermodynamic simulations to demonstrate that the trisulfur radical ion $S_3^{\bullet-}$ forms very stable and soluble complexes both with Pt^{II} and Pt^{IV} in sulfur-bearing aqueous solution at elevated temperatures (~300°C). These novel Pt-bearing species enable (re)mobilization, transfer, and focused precipitation of platinum up to 10,000 times more efficiently than any other common inorganic ligand such as hydroxide, chloride, sulfate or sulfide. Our results imply a far more important, than believed so far, contribution of sulfur-bearing hydrothermal fluids to PGE transfer and accumulation in the Earth’s crust. This discovery challenges traditional models of PGE economic concentration from silicate and sulfide melts, and provides new possibilities for resource prospecting in hydrothermal shallow-crust settings. The exceptionally high capacity of the $S_3^{\bullet-}$ ion to bind platinum may also offer new routes for PGE selective extraction from ore and hydrothermal synthesis of noble metal nanomaterials.

Significance Statement (118 words): Platinum group elements (PGE) are highly valued by many industrial applications, serve as important geochemical tracers of planetary processes, and are among eagerly sought natural resources of critical trace metals. We show here that aqueous sulfur-bearing fluids play a far more important role, than believed, in many natural and technological processes in which PGE are involved. This role is essentially ensured by the radical sulfur ion $S_3^{\bullet-}$ that forms extremely stable and soluble complexes both with Pt^{II} and Pt^{IV}. By enabling enhanced dissolution, transport and precipitation of Pt, these species may be key players in PGE transfer, fractionation, and accumulation in the Earth’s crust. They may also offer novel opportunities for optimizing ore processing and nanomaterial synthesis.

Main Text

Introduction

The increasing use of platinum in high-technology fields spanning from the automotive and petrochemical industries to pharmaceutics and nanomaterials, combined with its scarcity in nature (average Pt content in upper continental crust rocks is ~0.5 ng/g), makes Pt a highly valued commodity and eagerly sought natural resource (1-3). Currently assessed georessources of platinum group elements (PGE) are rare and mostly occur in mafic magmatic settings where PGE are concentrated in Fe-Ni-Cu sulfide minerals and melts (2-5). Their formation models are built on purely magmatic differentiation including fractional crystallization and sulfide-silicate partitioning and currently lack a robust assessment of the role of aqueous fluids. Indeed, systematic findings of inclusions of fluids and hydrous minerals in giant PGE magmatic deposits such as Bushveld, Norilsk, Sudbury (6-8) and in PGE-enriched mantle-derived rocks and lavas (9, 10) point to the potential role of post-magmatic aqueous fluids in PGE transfer and redistribution. Furthermore, there is multiple evidence of remobilization and concentration of Pt, as well as other PGE, in various low-to-moderate temperature (200–500°C) hydrothermal environments such as porphyry Cu-Au-Mo and metamorphic and sedimentary-hosted Au deposits, black shales, and serpentinites (4, 11), with Pt concentrations 1000 times its average crustal abundance, making such settings potentially exploitable for PGE. Therefore, knowledge of Pt chemical speciation and solubility in the hydrothermal fluid phase is required to quantify the formation and distribution of Pt resources in nature, to use PGE as geochemical tracers of Earth formation and evolution (e.g., 9, 10), as well as to optimize the rapidly growing Pt use in technological processes involving both aqueous and organic solvents (e.g., 1, 12-14).

Paradoxically, existing data on aqueous complexes of divalent Pt^{II}, which is a typical oxidation state of platinum in nature, with most common inorganic ligands such as chloride (Cl^-), sulfate (SO_4^{2-}), and hydroxide (OH^-) (15-17) yield far too small metal aqueous contents (<0.1 ng/g) in equilibrium with Pt-bearing mineral phases to account for the observed Pt mobility in most fluids below the magmatic-hydrothermal transition (<600–700°C). Such fluids, produced by magma degassing or metamorphism or circulating in sedimentary basins, are commonly near-neutral (4<pH<8), moderately saline (<20 wt% NaCl), and often sulfur-bearing (up to 1–3 wt% S) containing both sulfide and sulfate. Because of the high chemical affinity of Pt for reduced sulfur (18), hydrogen sulfide (HS^-) complexes are more plausible agents to transport Pt by such fluids. However, the reported data on their thermodynamic stability and the resulting solubility of Pt sulfide solids are highly controversial, spanning over almost 4 orders of magnitude, from <0.1 ng/g Pt in reduced H_2S-dominated fluids (19-21) to >1000 ng/g Pt in oxidized sulfide/sulfate-bearing fluids (22). Such discrepancies call upon complexes other than sulfide (and sulfate) and/or metal oxidation states other than Pt^{II} to account for platinum solubility.

The current speciation models of PGE in aqueous media ignore, in particular, the trisulfur radical ion, $S_3^{\bullet-}$, well-known in sulfur non-aqueous chemistry (23) and stable across a very wide temperature (T) and pressure (P) range of magmatic-to-epithermal sulfate/sulfide-bearing fluids (24-28). Moreover, this ligand was recently shown to bind to gold greatly enhancing the efficiency of Au supply to hydrothermal-magmatic porphyry and metamorphic ore deposits associated with subduction zone settings which commonly involve S-rich fluids (29). To quantify the effect of $S_3^{\bullet-}$ on Pt behavior in typical hydrothermal fluids, we used in situ X-ray absorption spectroscopy (XAS, including both near-edge structure or XANES, and extended fine structure or EXAFS) that provides a direct fingerprint of metal redox, coordination and ligand identity. The spectroscopic

data were combined with solubility measurements and quantum-chemistry and thermodynamic modeling of Pt speciation in aqueous sulfide/sulfate/$S_3^{\bullet-}$ solutions saturated with platinum sulfide solid PtS(s) at 275–300°C and 500–700 bar (*SI Appendix*).

Results

Platinum L_3-edge XANES spectra of $S_3^{\bullet-}$ bearing solutions show a systematic evolution as a function of pH and redox (expressed in $\log_{10}$ (bars) scale relative to the conventional hematite-magnetite f_{O2} mineral buffer, HM, Fig. 1*A*). Spectra of the near-neutral (pH 5.9 at 275°C) and relatively reduced (HM–0.2) solution are close to that of $Pt^{II}S$(s) both in energy position and amplitude, fully consistent with divalent Pt^{II} coordinated by 4 nearest S atoms in a square-planar geometry. By contrast, for more acidic and oxidized compositions, the spectra show a systematic shift to higher energies along with an increase in the white-line amplitude (Fig. 1*A*), indicating a change to higher Pt oxidation state and coordination, which would be closer to those of $Pt^{IV}S_2$(s) in which Pt is octahedrally coordinated by 6 S atoms. This trend is confirmed by quantum-chemistry simulations of XANES spectra (*SI Appendix*) by considering complexes with HS^- and $S_3^{\bullet-}$ ligands of square-planar and octahedral coordination geometry typical for Pt^{II} and Pt^{IV} compounds, respectively (18). The spectrum from the HM–0.2 solution closely resembles the simulation for square-planar $Pt^{II}(HS)_2(S_3)_2^{2-}$, whereas the spectrum from the HM+0.8 solution is best matched by octahedral $Pt^{IV}(HS)_3(H_2O)(S_3)_2^-$ (Fig. 1*B*). In contrast, none of the experimental spectra resembles the simulation for $Pt^{II}(HS)_4^{2-}$ (Fig. 1*B*) or other analogous $[Pt^{II}(HS)_n(H_2O)_{4-n}^{2-n}]$-type species commonly adopted in the literature (19-21), thus strongly supporting the predominance of new $[S_3^{\bullet-}]$-type species at our conditions.

These findings are fully supported by the EXAFS data that show a systematic increase of the first-shell mean Pt-S distance (from 2.32 to 2.36 ± 0.007 Å, 2 SD), and coordination number (from 4 to 5 ± 0.5 S atoms, 2 SD), from the most reduced and least acidic (HM–0.2, pH 5.9) to the most oxidized and most acidic (HM+0.8, pH 4.9) solutions, along with the presence of 2±1 second-shell S atoms at 3.50±0.02 Å in the second Pt shell of all solutions (*SI Appendix*, Figs. S2-S4; Table S1). Oxygen neighbors that may stem from OH groups or H_2O molecules in the Pt nearest atomic shell, were found to be below the detection limit of ≤1 O atom (*SI Appendix*). The amplitude of changes of the 1st shell Pt-S distances (>0.04 Å) and coordination numbers (from 4 to 5) with f_{O2} and pH (*SI Appendix*, Fig. S4) definitely implies a mixture of different species, and cannot be explained by the presence of only divalent Pt^{II}-S complexes, which are commonly square planar and have a very narrow range of Pt-S_4 distances (2.30–2.32 Å; e.g., refs. 18, 30). Therefore, our findings are more consistent with the presence of both Pt^{II} and Pt^{IV} species in variable proportions in solution. Furthermore, the detection of 2nd shell S atoms provides compelling evidence for the presence of the $S_3^{\bullet-}$ ligand in both types of Pt complexes.

Using these key constraints from in situ spectroscopy, we applied thermodynamic modeling to the two sets of PtS(s) solubility data, one obtained simultaneously with the XAS spectra at 275°C/700 bar (Figs. S1*A*, S5, Table S1) and the other from batch-reactor measurements at 300°C/500 bar conducted within similar ranges of redox, pH and solution composition (Figs. S1*B*, 2, Table S2). Both datasets were found to be consistent with the formation of two complexes, $Pt^{II}(HS)_2(S_3)_2^{2-}$ and $Pt^{IV}(HS)_3(H_2O)(S_3)_2^{-}$, that control the solubility at near-neutral pH/more reducing conditions and acidic pH/more oxidizing conditions, respectively (Fig. 2):

$$PtS(s) + H_2S(aq) + 2\ S_3^{\bullet-} = Pt^{II}(HS)_2(S_3)_2^{2-} \quad \textbf{[1]}$$

$$PtS(s) + 2\ H_2S(aq) + 2\ S_3^{\bullet-} + H^+ + 0.5\ O_2(g) = Pt^{IV}(HS)_3(H_2O)(S_3)_2^{-} \quad \textbf{[2]}$$

Fig. 2 shows that the presence of relatively minor concentrations of $S_3^{\bullet-}$ in solution (~10 mmol, versus >100 mmol of H_2S/HS^-) leads to 4 to 5 order-of-magnitude enhancement of PtS(s) solubility compared to predictions for the commonly assumed hydrogen sulfide complexes from literature data obtained using reduced H_2S-dominated solutions (19, 21). The relative affinities of Pt^{II} to the $S_3^{\bullet-}$ and HS^- ligands may be evaluated using a symmetrical ligand exchange reaction between $Pt^{II}(HS)_2(S_3)_2^{2-}$ and the $Pt(HS)_4^{2-}$ complex of the same electric charge and coordination:

$$Pt(HS)_4^{2-} + 2\ S_3^{\bullet-} = Pt(HS)_2(S_3)_2^{2-} + 2\ HS^- \qquad \textbf{[3]}$$

The value of the reaction **[3]** equilibrium constant at 300°C and 500 bar is $10^{8.7}$ as derived by combining the data of this study (Tables S3 and S5) and those for $Pt(HS)_4^{2-}$ from ref. (19). This value means that the affinity of Pt^{II} for one $S_3^{\bullet-}$ ligand is at least ~10^4 greater than for one HS^- ligand. Such remarkable affinity to $S_3^{\bullet-}$ may be related to a favorable combination of the electronic configurations of both Pt^{II} having two empty 5d shell orbitals ($[Xe]4f^{14}5d^86s^0$) and the radical $S_3^{\bullet-}$ ion having an unpaired electron to fill these orbitals in a chemical bond, coupled with favorable steric factors yielding a highly stable symmetrical complex geometry with 2 $S_3^{\bullet-}$ ligands in trans-position (Fig. 1*B*). Remarkably, the affinities of aurous gold (Au^I) for $S_3^{\bullet-}$ and HS^- are very similar as attested by an equilibrium constant of ~1 for an analogous ligand exchange reaction: $Au(HS)_2^- + S_3^{\bullet-} = Au(HS)(S_3)^- + HS^-$, studied across a temperature range of 200–500°C (29). Compared to Pt^{II} or Pt^{IV}, Au^I has its 5d shell filled ($5d^{10}$), which may render bonding with the different sulfur ligands less specific. Furthermore, the 4 and 6-coordinated geometries of Pt offer more flexibility and less steric strain for binding to 2 $S_3^{\bullet-}$ ligands, compared to Au^I whose stable coordination is limited to quasi-linear geometries (L-Au-L, e.g., refs. 29, 33). These tendencies are also in good agreement with the generally more chalcophile (i.e. sulfur loving) character of Pt that forms far more stable (poly)sulfide solid phases than those formed by Au (e.g., 18, 30). The equilibrium

constant values derived for reactions **[1]** and **[2]** (Table S5) allow Pt solubility predictions across the wide compositional range of natural and technological S-bearing hydrothermal fluids (Fig. 3).

Discussion and Applications

The discovery of stable soluble platinum-trisulfur ion complexes in aqueous fluids offers new applications in geoscience, chemistry and material science.

First, the large enhancement of Pt solubility in hydrothermal ore-forming fluids in the presence of $S_3^{\bullet-}$ explains the multiple cases of PGE enrichment in a variety of hydrothermal sulfide deposits of common metals (Cu, Mo, Zn, Au, Ag), which may become a novel economic source of platinoids in near future. Our predictions of Pt solubility (Fig. 3) show that μg/g levels of metal concentrations may easily be transported by typical epithermal fluids at temperatures around 300°C. Our predictions are in marked contrast with former models based on ‘traditional’ sulfide and chloride ligands that account for less than ng/g levels of Pt in such fluids. Consequently, breakdown of $S_3^{\bullet-}$ within rather narrow S concentration (0.1–1 wt%), pH (3–7) and f_{O2} (HM±1) windows upon the evolution of a S-rich hydrothermal fluid would yield focused Pt precipitation in high tenors from a fluid volume 10^3 to 10^5 times smaller than would be required to precipitate the same platinum amount if the [Pt-S_3] complexes were ignored. Compared to gold, whose speciation is dominated by hydrogen sulfide complexes in most hydrothermal solutions of near-neutral pH below 350°C ($Au(HS)_2^-$; Fig. 3*D*) because of the much greater abundance of the HS^-/H_2S ligands than $S_3^{\bullet-}$, platinum mobility is far more strongly enhanced in the presence of even small amounts of $S_3^{\bullet-}$. Therefore, this ligand may control the fractionation of PGE from Au as well as other more common metals such as Cu, Zn, Pb, or Ni. These metals have a weaker chemical affinity to $S_3^{\bullet-}$

and their speciation is dominated by complexes with far more abundant chloride in most hydrothermal fluids (29).

Second, on a larger mantle-crust scale, S-bearing aqueous fluids may play a far more important role in PGE behavior than believed. Even though our exploratory data set does not currently allow extrapolations to higher, closer to magmatic, temperatures, the growing stability of $S_3^{\bullet-}$ as well as of its higher-temperature (>500°C) counterpart $S_2^{\bullet-}$ (26, 28), suggests that both radical ions may play a key role in PGE mobility in hydrothermal-magmatic systems. As a result, the radical ions may promote PGE transfers from deep magmas or metamorphic rocks in subduction zones to aqueous fluids and their massive transport up to shallow crust settings, thereby explaining the observed PGE enrichment in gold and base metal porphyry-epithermal deposits, black-shale sedimentary environments, and serpentinites. Our findings of stable PGE complexes with $S_3^{\bullet-}$, if further confirmed across a wider *T-P* range, may shift the long-standing paradigms on PGE deposit formation by purely magmatic processes, in the light of multiple evidence of aqueous fluid presence (6-8, 11). Quantifying the role of such S-bearing fluids requires more systematic data on PGE interactions with the sulfur radical ions over the magmatic-hydrothermal *T-P* range. Our results demonstrating a strong Pt enrichment in S-bearing fluids, in which the aqueous sulfate and sulfide forms of sulfur coexist, may offer novel perspectives in the exploration of alternative PGE economic sources in hydrothermal settings that host both sulfate and sulfide mineral assemblages. Furthermore, our study points to an important role of slab-derived fluids under redox conditions of the sulfate-sulfide coexistence common in subduction zones and favoring the abundance of $S_3^{\bullet-}$ and $S_2^{\bullet-}$ (e.g., 28). Such fluids, often enriched in sulfur, may be capable of selectively mobilizing Pt and, by analogy, electronically similar Pd^{II} and Ir^{I}, from the mantle wedge. On the other hand, other, less

chalcophile PGE such as Ru, Rh or Os, generally having weaker affinities for soft ligands like (poly)sulfides (18), would be much less affected. These differences in the affinity to $S_3^{\bullet-}$ may thus induce fluid-mineral fractionations among different PGE thereby impacting their both elemental and isotopic signatures in mantle-derived rocks that are widely used as geochemical tracers of planetary accretion and core-mantle evolution (e.g., 9, 10).

Third, the discovery of highly soluble $S_3^{\bullet-}$ complexes with both Pt^{II} and Pt^{IV} may open new routes for hydrothermal synthesis of PGE-based nanomaterials increasingly used in catalysis, medicine, and electronics. Trisulfur ion may offer an interesting alternative to organic thiolate ligands currently used as precursors in the synthesis of Au and Pt nanoparticles and their stabilization in solution (31, 32). Furthermore, the specific solubility pattern of PtS(s) and, by analogy, of Pt metal as a function of solution pH and redox potential, passing through a maximum at slightly acidic pH and an H_2S/SO_4 ratio of ~4, corresponding to the maximum of $S_3^{\bullet-}$ abundance (Fig. 3), may be explored for optimizing Pt nanoparticle preparation and functionalization both through reduction/oxidation and acidification/basification. Such unique solubility dependence thus offers greater flexibility and a larger redox, pH and temperature window for synthesis protocols both in aqueous or organic solvents than those currently based on H_2 reduction of Pt^{II} chloride or thiolate complexes unstable at elevated temperatures (e.g., 12-14). Our findings thus extend the choice of S-ligands and provide more potential for tuning the molecular mechanisms that control the shape, atomicity, structure, and resulting reactivity of the formed nanoparticles of noble metals.

Methods Summary (See *SI Appendix* for detailed description of experimental and model systems, methods, and uncertainties)

X-Ray Absorption Spectroscopy and Solubility Measurements. Platinum solubility and chemical molecular speciation were investigated in aqueous PtS(s)-saturated solutions of thiosulfate and elemental sulfur that yield variable equilibrium amounts of hydrogen sulfide (H_2S/HS^-), (hydrogen)sulfate (HSO_4^-/SO_4^{2-}) and $S_3^{\bullet-}$ ion, and provide redox and acidity (pH) buffering of the system (e.g., 29, 33). In situ X-ray absorption spectroscopy (XAS) measurements at Pt L_3-edge (11.564 keV) were performed at BM30-FAME beamline of the European Synchrotron Radiation Facility (ESRF, Grenoble, France), using a hydrothermal apparatus developed at the Néel Institute. This setup enables simultaneous acquisition of high-quality fluorescence spectra from dilute solutions (down to 0.1 mmol Pt) to extract ligand identity, molecular structure and metal redox state and to directly determine the total dissolved Pt concentration (33). Measurements were conducted at 275°C and 700 bar. The XAS experiments were complemented by batch-reactor measurements of PtS(s) solubility at similar conditions (300°C, 500 bar) using hydrothermal reactors allowing controlled sampling or quenching of the fluid that was processed and analyzed using recent protocols developed for trace metals in S-rich solutions (20).

Molecular simulations and XANES spectra modeling. Both static Density Functional Theory (DFT) and First Principles Molecular Dynamics (FPMD) simulations of the geometries and interatomic distances of selected [Pt-HS-S_3]-type complexes were performed following approaches developed for a similar Au-HS^-/H_2S-$S_3^{\bullet-}$ system (29). The calculated molecular structures were compared with experimental XAS-derived distances and coordination numbers to better constrain the stoichiometry of complexes. In addition, XANES spectra of such complexes were simulated using the FDMNES package (*SI Appendix*) and compared with the experimental spectra to further constrain the Pt coordination and oxidation state in the fluid phase.

Thermodynamic analysis of platinum speciation and solubility. Platinum solubility in experimental solutions was modeled in terms of dominant [Pt-HS-S_3] complexes using the constraints imposed by the spectroscopic and molecular data, and based on available robust thermodynamic properties of aqueous sulfur species including $S_3^{\bullet-}$ (*SI Appendix*, Table S3). The derived stoichiometries and formation constants for the two dominant Pt^{II} and Pt^{IV} complexes (reactions **[1]** and **[2]**) are consistent with the whole set of experimental data. The generated reaction constants values allow PtS(s) solubility to be predicted in S-bearing epithermal fluids (~300°C, 500 bar) as a function of pH, oxygen fugacity and total sulfur content with an overall precision of better than ±1 order of magnitude (*SI Appendix*).

Acknowledgements

This work was funded by the French National Research Agency (grant RadicalS, ANR-16-CE31-0017), the Institut Carnot ISIFoR (grant OrPet), and the Centre National de la Recherche Scientifique (grant PtS3, MétalloMix-2021). We acknowledge the European Synchrotron Radiation Facility (ESRF) for access to beam time and infrastructure, and the Grand Equipement National for Calcul Intensif (GENCI) and the Institut du Développement et des

Ressources en Informatique Scientifique (IDRIS) for access to computing facilities. The FAME-UHD project is supported by the French Grand Emprunt EquipEx (EcoX ANR-10-EQPX-27-01), the CEA-CNRS CRG consortium and the INSU-CNRS. The Cluster of Excellence MATISSE led by Sorbonne University is supported by the ANR Investissement d’Avenir (ANR-11-IDEX-0004-02). A. Colin, I. Kieffer, E. Lahera, O. Proux, and A. Seitsonen are acknowledged for help with the synchrotron experiments and FPMD calculations. Special thanks go to A-M. Cousin for assistance with figure layout and to Y. Joly for advice on XANES modeling. Comments of the Editor and two anonymous referees greatly improved this article.

References

1. V. W. W. Yam, Behind platinum’s sparkle. *Nat. Chem.* **2**, 790 (2010).

2. G. Gunn, *Critical Metals Handbook*. Wiley (2014).

3. J. M. Brenan, The platinum-group elements: “admirably adapted” for science and industry. *Elements* **4**, 227−232.

4. J. E. Mungall (ed.), Exploration for platinum-group elements deposits. *Min. Assoc. Canada Short Course* **35**, 1−494 (2005).

5. S-J. Barnes, E. M. Ripley, Highly siderophile and strongly chalcophile elements in magmatic deposits. *Rev. Mineral. Geochem*. **81**, 725−774 (2016).

6. C. G. Ballhaus, E.F. Stumpfl, Sulfide and platinum mineralization in the Merensky Reef: evidence from hydrous silicates and fluid inclusions. *Contrib. Mineral. Petrol*. **94**, 193−204 (1986).

7. S. Arai, M. Miura, Formation and modification of chromitites in the mantle. *Lithos* **264**, 277−295 (2016).

8. A. Boudreau, *Hydromagmatic Processes and Platinum-group Elements in Layered Intrusions*. Cambridge Univ. Press, 1−275 (2019).

9. M. Rehkämper, A. N. Halliday, D. Barfod, J. G. Fitton, J. B. Dawson, Platinum-group element abundance patterns in different mantle environments. *Science* **278**, 1595−1598 (1997).

10. A. Luguet, D. G. Pearson, G. M. Nowell, S. T. Dreher, J. A. Coggon, Z. V. Spetsius, S. W. Parman, Enriched Pt-Re-Os isotope systematics in plume lavas explained by metasomatic sulfides. *Science* **319**, 453−456 (2008).

11. S. A. Wood, The aqueous geochemistry of the platinum-group elements with applications to ore deposits. In: The Geology, Geochemistry, Mineralogy and Mineral Beneficiation of Platinum-Group Elements, ed. L.J. Cabri, *Canadian Institute of Mining, Metallurgy and Petroleum Special Volume* **54**, 211–250 (2002).

12. T. S. Ahmadi, Z. L. Wang, T. C. Green, A. Hendlein, M. A. El-Sayed, Shape-controlled synthesis of colloidal platinum nanoparticles. *Science* **272**, 1924−1926 (1996).

13. L. Chong et al., Ultralow-loading platinum-cobalt fuel cell catalysts derived from imidazolate frameworks. *Science* **362**, 1276−1281 (2018).

14. I. Lee, R. Morales, M. A. Albiter, F. Zaera, Synthesis of heterogeneous catalysts with well shaped platinum particles to control reaction selectivity. *Proc. Natl. Acad. Sci. U.S.A.* **105**, 15241−15246 (2008).

15. D. C. Sassani, E .L. Shock, Solubility and transport of platinum-group elements in supercritical fluids: Summary and estimates of thermodynamic properties for ruthenium, rhodium, palladium, and platinum solids, aqueous ions, and complexes to 1000°C and 5 kbar. *Geochim. Cosmochim. Acta* **62**, 2643−2671 (1998).

16. E. F. Bazarkina, G. S. Pokrovski, J.-L. Hazemann, Structure, stability and geochemical role of palladium chloride complexes in hydrothermal fluids. *Geochim. Cosmochim. Acta* **146**, 107−131 (2014).

17. B. R. Tagirov, O. N. Filimonova, A. L. Trigub, N. A. Akinfiev, M. S. Nickolsky, K. O. Kvashnina, D. A. Chareev, A. V. Zotov, Platinum transport in chloride-bearing fluids and melts: insights from in-situ X-ray absorption spectroscopy and thermodynamic modeling. *Geochim. Cosmochim. Acta* **254**, 86−101 (2019).

18. F. A. Cotton, G. Wilkinson, C. A. Murillo, M. Bochmann, *Advanced Inorganic Chemistry*, 6th Edition, Wiley, Chichester (1999).

19. C. H. Gammons, M. S. Bloom, Experimental investigation of the hydrothermal geochemistry of platinum and palladium: II. The solubility of PtS and PdS in aqueous sulfide solutions to 300°C. *Geochim. Cosmochim. Acta* **57**, 2451−2467 (1993).

20. M. A. Kokh, N. N. Akinfiev, G. S. Pokrovski, S. Salvi, D. Guillaume, The role of carbon dioxide in the transport and fractionation of metals by geological fluids. *Geochim. Cosmochim. Acta* **197**, 433−466 (2017).

21. O. N. Filimonova, B. R. Tagirov, A. V. Zotov, N. N. Baranova, Y. V. Bychkova, D. A. Tyurin, D. A. Chareev, M. S. Nickolsky, The solubility of cooperate PtS(cr) at 25–450°C, P_{sat}–1000 bar and hydrosulfide complexing of platinum in hydrothermal fluids. *Chem. Geol*. **559**, 119968 (2021).

22. P. Pan, S. A. Wood, Solubility of Pt and Pd sulfides and Au metal in aqueous bisulfide solutions. II. Results at 200° to 350°C and saturated vapor pressure. *Min. Deposita* **29**, 373−390 (1994).

23. T. Chivers, P. J. W. Elder, Ubiquitous trisulfur radical ion: fundamentals and applications in materials science, electrochemistry, analytical chemistry and geochemistry. *Chem. Soc. Rev.* **42**, 5996−6005 (2013).

24. G. S. Pokrovski, L. S. Dubrovinsky, The S_3^- ion is stable in geological fluids at elevated temperatures and pressures. *Science* **331**, 1052−1054 (2011).

25. N. Jacquemet, D. Guillaume, A. Zwick, G. S. Pokrovski, In situ Raman spectroscopy identification of the S_3^- ion in S-rich hydrothermal fluids from synthetic fluid inclusions. *Amer. Miner.* **99**, 1109−1118 (2014).

26. G. S. Pokrovski, J. Dubessy, Stability and abundance of the trisulfur radical ion S_3^- in hydrothermal fluids, *Earth Planet. Sci. Lett*. **411**, 298−309 (2015).

27. G. Barré, L. Truche, E. F. Bazarkina, R. Michels, J. Dubessy, First evidence of the trisulfur radical ion S_3^- and other sulfur polymers in natural fluid inclusions. *Chem. Geol*. **462**, 1−14 (2017).

28. A. Colin, C. Schmidt, G. S. Pokrovski, M. Wilke, A. Y. Borisova, M. J. Toplis, *In situ* determination of sulfur speciation and partitioning in aqueous fluid-silicate melt systems. *Geochem. Persp. Let*. **14**, 31–35 (2020).

29. G. S. Pokrovski, M. A. Kokh, D. Guillaume, A. Y. Borisova, P. Gisquet, J.-L. Hazemann, E. Lahera, W. Del Net, O. Proux, D. Testemale, V. Haigis, R. Jonchière, A.P. Seitsonen, G. Ferlat, R. Vuilleumier, A. M. Saitta, M.-C. Boiron, J. Dubessy, Sulfur radical species form gold deposits on Earth. *Proc. Natl. Acad. Sci. U.S.A.* **112**, 13484–13489 (2015).

30. ICSD - *Inorganic Crystal Structure Database*, FIZ Karlsruhe, 2021, https://icsd.products.fiz-karlsruhe.de/ [accessed 18 May 2021].

31. T. Imaoka, Y. Akanuma, N. Haruta, S. Tsuchiya, K. Ishihara, T. Okayasu, W-J. Chun, M. Takashashi, K. Yamamoto, Platinum clusters with precise numbers of atoms from preparative-scale catalysis. *Nat. Comm*. **8**, 688 (2017).

32. H. Häkkinen, The gold-sulfur interface at the nanoscale. *Nat. Chem*. **4**, 443–455 (2012).

33. G. S. Pokrovski, B. R. Tagirov, J. Schott, J-L., Hazemann, O. Proux, A new view on gold speciation in sulfur-bearing hydrothermal fluids from in-situ X-ray absorption spectroscopy and quantum-chemical modeling, *Geochim. Cosmochim. Acta* **73**, 5406–5427 (2009).

Figure captions

Fig. 1. Platinum L_3-edge XANES spectra of S-bearing aqueous solutions in equilibrium with PtS(s) at indicated pH and oxygen fugacity (relative to the conventional hematite-magnetite mineral buffer, HM) recorded at 275°C and 700 bar and compared with reference compounds (*A*) and quantum-chemistry simulated XANES spectra of representative [Pt-HS-S_3]-type complexes with structures optimized using molecular modeling (*B*). Vertical dashed lines are an eye guide to indicate differences in the experimental spectra (*A*) with changes of pH and oxygen fugacity, and (*B*) among the calculated spectra of the shown Pt^{II} and Pt^{IV} species (see *SI Appendix*, Fig. S1*A* and Table S1 for solution composition and speciation).

Fig. 2. Direct evidence for platinum-trisulfur ion complexes from PtS(s) solubility measurements in aqueous thiosulfate solutions as a function of pH and $S_3^{\bullet-}$ ion concentration at 300°C and 500 bar. Thiosulfate irreversibly breaks down on heating by providing sulfate, sulfide and $S_3^{\bullet-}$ ion (*SI Appendix*). Symbols represent the measured Pt concentrations (error bars = 2 SD); solid red line shows the predicted total Pt solubility according to the speciation model of this study that includes the two indicated Pt^{II} and Pt^{IV} complexes with $S_3^{\bullet-}$ and HS^- ligands (dotted blue and purple lines); dashed green curve shows the sum of concentrations of $Pt(HS)_n^{2-n}$ complexes from the literature, where n = 2, 3 or 4 (19, 21); dashed black curves indicate the free concentration of the two ligands, HS^- and $S_3^{\bullet-}$. The break in the species curve pattern at pH ~5 reflects the onset of molten sulfur (S_{liq}) formation at more acidic pH (Table S3 for data sources and Fig. S1*B* for details on S aqueous speciation).

Fig. 3. Platinum dissolved concentration in equilibrium with PtS(s) in hydrothermal fluid at 300°C and 500 bar and its comparison with gold as a function of (*A*) total dissolved S concentration at pH ~5 and f_{O2} buffered by sulfide-sulfate equilibrium with $(H_2S)_{tot}$:$(SO_4)_{tot}$ molal ratio of 4:1 corresponding to the maximum of $S_3^{\bullet-}$ abundance; (*B*) oxygen fugacity corresponding to common redox buffers, QFM – quartz-fayalite-magnetite, NNO – nickel-nickel oxide, PPM – pyrite-pyrrhotite-magnetite, and HM – hematite-magnetite; (*C*) fluid acidity, pH = $-\log_{10} a(H^+)$ at f_{O2} buffered by sulfide-sulfate equilibrium (H_2S:SO_4 = 4:1); (*D*) in equilibrium with gold metal as a function of pH at the conditions identical to (*C*). In all panels, the curves denote the concentrations of $S_3^{\bullet-}$ (blue, in μg/g of S, same scale as for Pt and Au), sum of known Pt/Au-Cl, Pt/Au-HS, Pt-SO_4 and Au-OH species (green) and the total Pt or Au solubility (red) including $Pt(HS)_2(S_3)_2^{2-}$ and $Pt(HS)_3(H_2O)(S_3)_2^-$ or $Au(HS)S_3^-$. The difference between the two latter curves (vertical pink arrow), corresponds to the contribution of [Pt-S_3^-]- or [Au-S_3^-]-type complexes. The thermodynamic properties of Au/Pt-Cl-HS-SO_4 species and other fluid constituents are from Table S3.

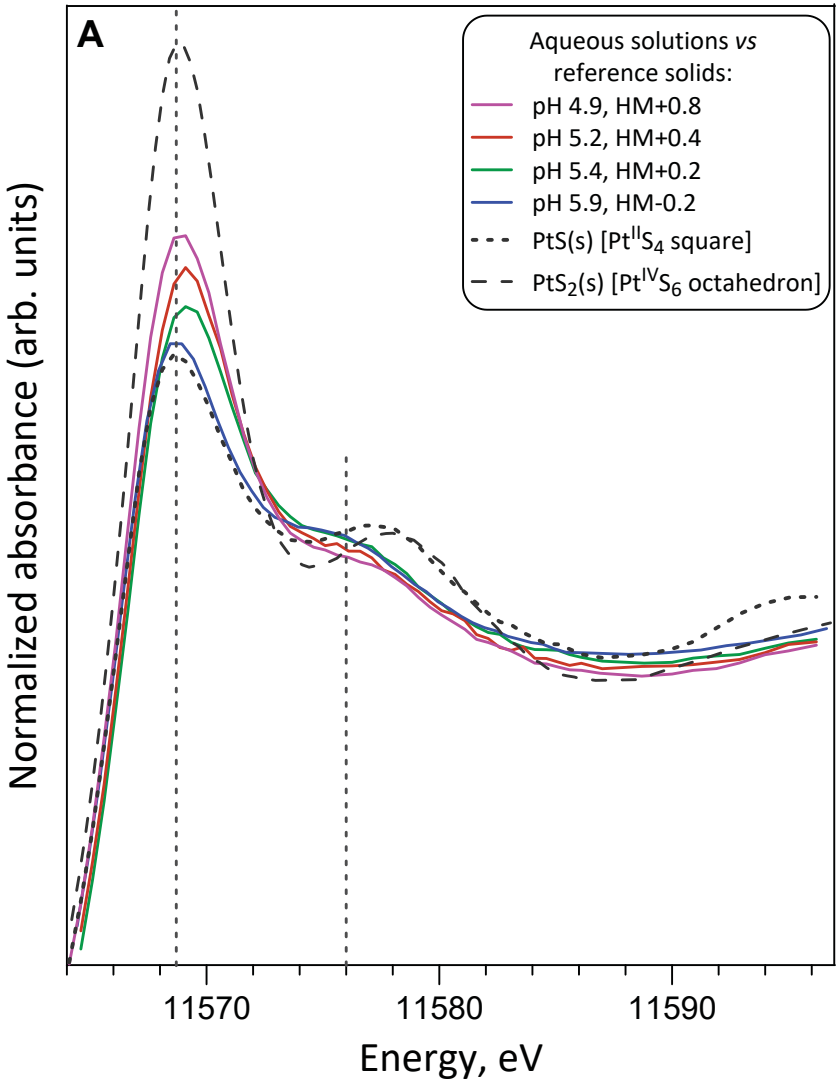
A
Aqueous solutions vs reference solids:
pH 4.9, HM+0.8
pH 5.2, HM+0.4
pH 5.4, HM+0.2
pH 5.9, HM-0.2
PtS(s) [Pt^II S4 square]
PtS2(s) [Pt^IV S6 octahedron]
Normalized absorbance (arb. units)
11570
11580
11590
Energy, eV

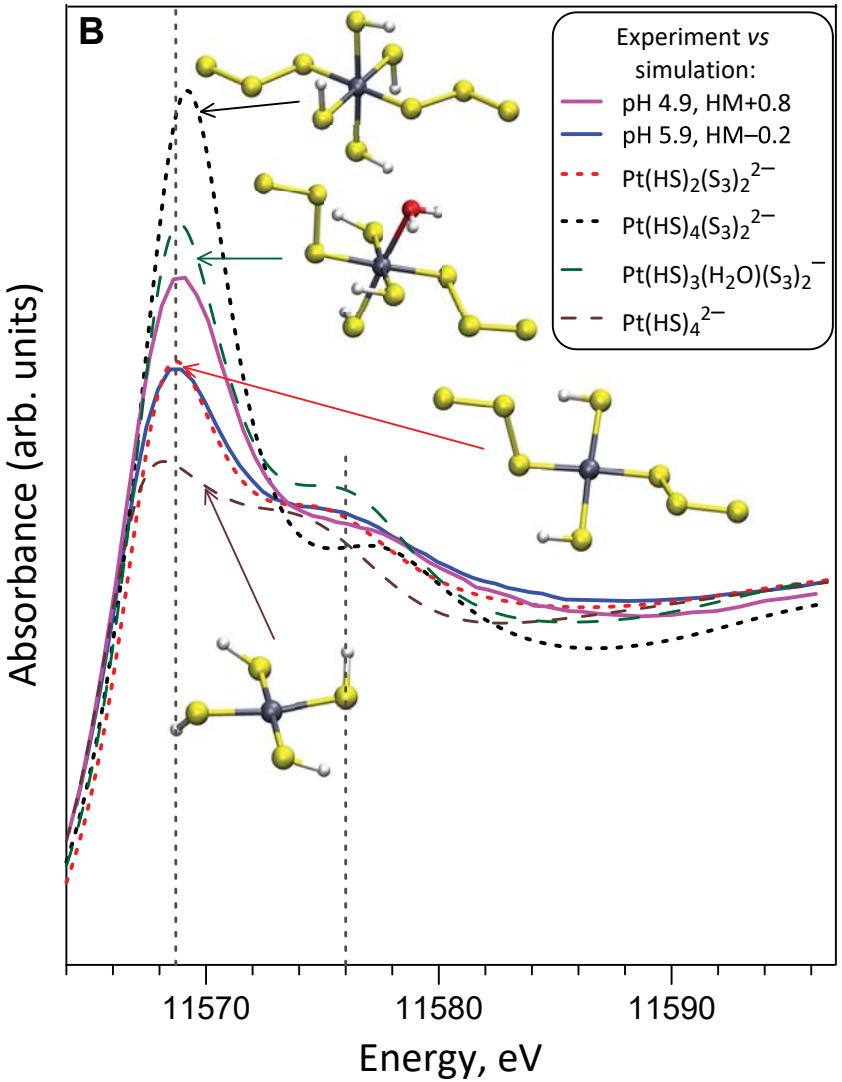
B
Experiment vs simulation:
pH 4.9, HM+0.8
pH 5.9, HM–0.2
Pt(HS)2(S3)2 2–
Pt(HS)4(S3)2 2–
Pt(HS)3(H2O)(S3)2 –
Pt(HS)4 2–
Absorbance (arb. units)
11570
11580
11590
Energy, eV

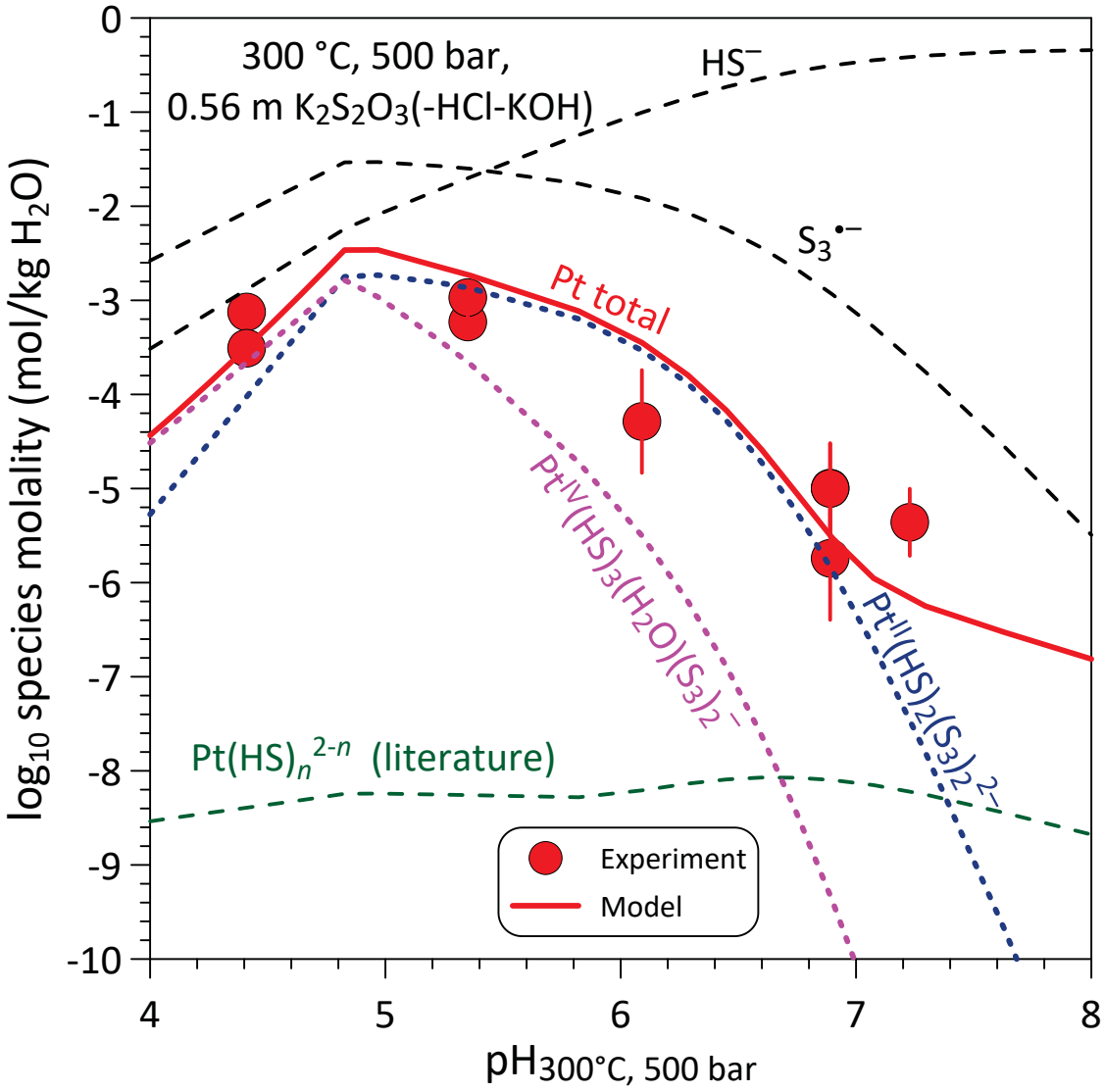
300 °C, 500 bar,
0.56 m K2S2O3(-HCl-KOH)
HS⁻
S3•⁻
Pt total
Pt^IV(HS)3(H2O)(S3)2⁻
Pt^II(HS)2(S3)2^2-
Pt(HS)n^2-n (literature)
Experiment
Model
log10 species molality (mol/kg H2O)
pH300°C, 500 bar
0
-1
-2
-3
-4
-5
-6
-7
-8
-9
-10
4
5
6
7
8

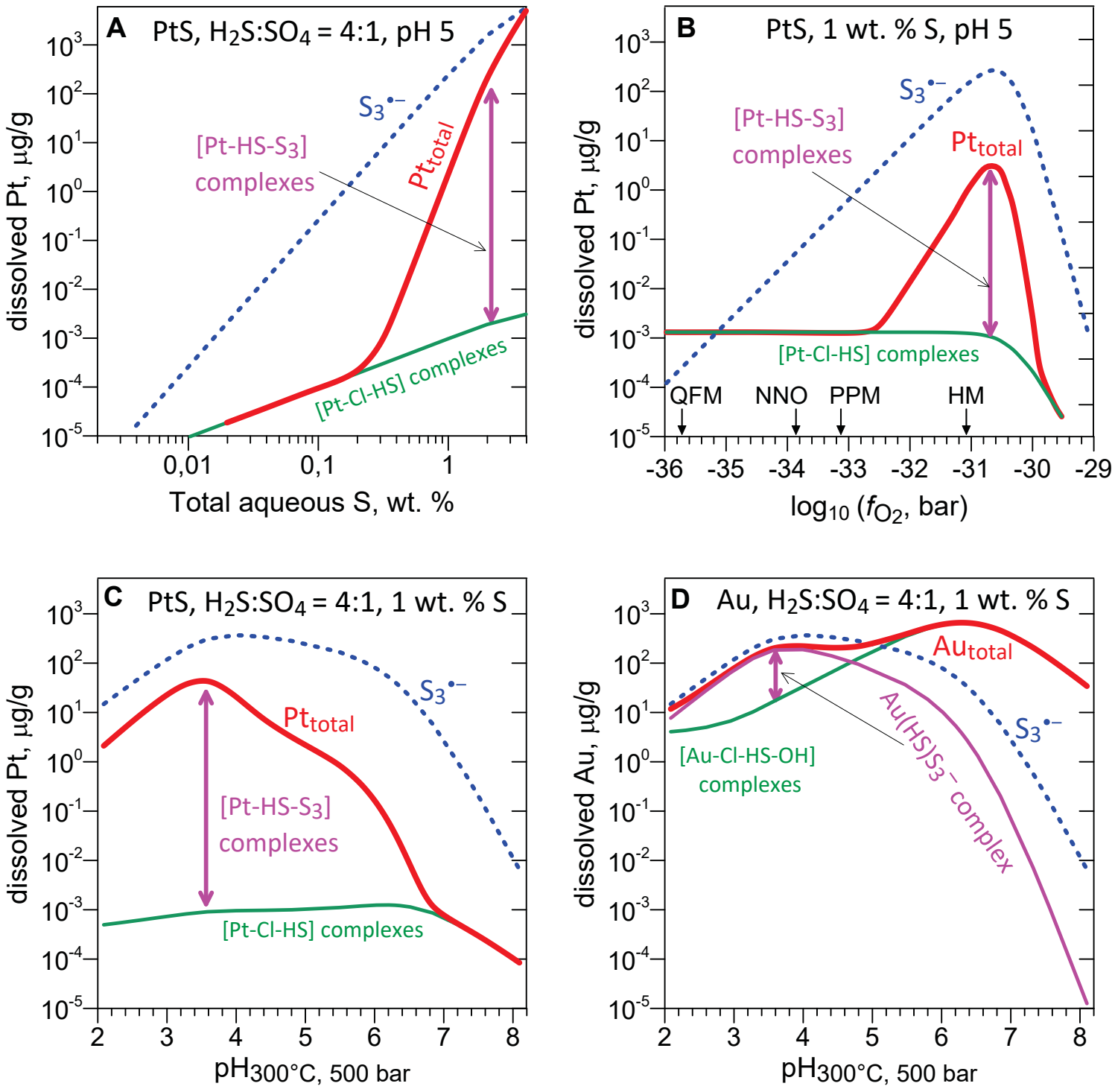
A
PtS, H2S:SO4 = 4:1, pH 5
S3•−
[Pt-HS-S3] complexes
Pttotal
[Pt-Cl-HS] complexes
dissolved Pt, µg/g
Total aqueous S, wt. %
B
PtS, 1 wt. % S, pH 5
S3•−
[Pt-HS-S3] complexes
Pttotal
[Pt-Cl-HS] complexes
QFM
NNO
PPM
HM
dissolved Pt, µg/g
log10 (fO2, bar)
C
PtS, H2S:SO4 = 4:1, 1 wt. % S
S3•−
Pttotal
[Pt-HS-S3] complexes
[Pt-Cl-HS] complexes
dissolved Pt, µg/g
pH300°C, 500 bar
D
Au, H2S:SO4 = 4:1, 1 wt. % S
Autotal
S3•−
[Au-Cl-HS-OH] complexes
Au(HS)S3− complex
dissolved Au, µg/g
pH300°C, 500 bar